

Supplementary Information

Insights into the Enhanced Electrochemical Sensing Behavior of Hydroquinone and Catechol Simultaneously Enabled by Ultrafine Layer CoP-NiCoP Heterostructure on Graphene Frameworks

Yanyan Zhu,^{a*}, Kai Kang^a, Juan Jia^a, Sen Wang^{b*}, Jing Wang^{a*}

a. School of Pharmaceutical Sciences, Key Laboratory of Innovative Drug Development and Evaluation, Hebei Medical University, Shijiazhuang, 050017, (P.R. China); *E-mail: zhuyanyan@hebmh.edu.cn; jingwang@home.ipe.ac.cn.

b. Institute of Coal Chemistry, Chinese Academy of Sciences, Taiyuan, 030001, (P.R. China); [E-mail: wangsen@sxicc.ac.cn](mailto:wangsen@sxicc.ac.cn).

KEYWORDS: Dihydroxybenzene isomers; electrochemical sensor; heterojunction, transition metal phosphide; ultrafine nanosheet; electrocatalytic activity.

This supplementary information containing **Experimental Section**, **Figs. S1-S10**, and **Table S1-S3**.

1. Experimental Section

1.1 Reagents

Glucose, sodium carbonate (Na_2CO_3), disodium hydrogen phosphate ($\text{Na}_2\text{HPO}_4 \cdot 2\text{H}_2\text{O}$), sodium hydroxide (NaOH), hydrochloric acid (HCl), and sodium dihydrogen phosphate ($\text{NaH}_2\text{PO}_4 \cdot 2\text{H}_2\text{O}$) were purchased from Yongda Chemical Reagent Co., Ltd (Tianjin, China). $\text{Ni}(\text{NO}_3)_2 \cdot 6\text{H}_2\text{O}$, $\text{Co}(\text{NO}_3)_2 \cdot 6\text{H}_2\text{O}$, $\text{K}_2[\text{Fe}(\text{CN})_6]$, $\text{K}_3[\text{Fe}(\text{CN})_6]$, catechol, hydroquinone, and sodium hypophosphite ($\text{NaH}_2\text{PO}_2 \cdot \text{H}_2\text{O}$) were obtained from Aladdin Bio-Chem Technology Co., LTD (Shanghai, China). Nafion were purchased from Sigma-Aldrich Co., LTD (Shanghai, China). This study uses the Millipore-Q water (18.2 M Ω cm) and analytical grades chemicals.

1.2 Synthesis of CoP-NiCoP/GFs

Synthesis of CoP-NiCoP/GFs: Firstly, the synthesis of GFs was through a fast pyrolysis the mixture of glucose and Na_2CO_3 process, and then washed and collected according to a previous report of our research group¹. Secondly, the precursor of $\text{Ni}_{0.25}\text{Co}_{0.75}$ layered hydroxide (LDH)/GFs were achieved through a modified facile co-precipitation process². Briefly, the GFs (20 mg) were dispersed in 50 mL ultrapure water containing the calculated quantity of $\text{Ni}(\text{NO}_3)_2 \cdot 6\text{H}_2\text{O}$ and

$\text{Co}(\text{NO}_3)_2 \cdot 6\text{H}_2\text{O}$ (the molar ratio of $\text{Ni}(\text{NO}_3)_2 \cdot 6\text{H}_2\text{O}$ to $\text{Co}(\text{NO}_3)_2 \cdot 6\text{H}_2\text{O}$ is 1:3), which sonicated for 1 h to absorb the Ni^{3+} and Co^{3+} on the surface of GFs. Then, NaOH (150 mg)/ Na_2CO_3 (100 mg) dissolved in 100 mL ultrapure water was added to the above suspension until the pH to 9 and aged under agitation at indoor temperature for 24 h to form $\text{Ni}_{0.25}\text{Co}_{0.75}$ LDH /GFs, and then the product was collected after centrifugation, repeatedly washed by ethanol, and dried at 40 °C in vacuum oven. As a comparison, the Co LDH /GFs, $\text{Ni}_{0.5}\text{Co}_{0.5}$ LDH /GFs, and $\text{Ni}_{0.25}\text{Co}_{0.75}$ LDH were achieved by adjusting the amount of $\text{Ni}(\text{NO}_3)_2 \cdot 6\text{H}_2\text{O}$ and $\text{Co}(\text{NO}_3)_2 \cdot 6\text{H}_2\text{O}$. Finally, different compositions of NiCo phosphides (e. g. CoP-NiCoP/GFs, NiCoP/GFs, CoP/GFs, and CoP-NiCoP) were achieved via phosphorization of $\text{Ni}_{0.25}\text{Co}_{0.75}$ LDH/GFs, $\text{Ni}_{0.5}\text{Co}_{0.5}$ LDH/GFs, Co LDH/GFs, and $\text{Ni}_{0.25}\text{Co}_{0.75}$ LDH composites at 350 °C for 2 h, respectively. Typically, the obtained hydroxide (0.2 g) put in the quartz tube center with NaH_2PO_2 (2.0 g) in the upriver section close to it. The furnace was subsequently heated to 350 °C and kept in N_2 atmosphere for 2 h.

1.3 Preparation of modified GCE electrode

GCE was pretreated by polishing with 0.05 μm Al_2O_3 , and then ultrasonic cleaning with water. The working electrode was fabricated via an easy drop-casting method. The as-prepared sample slurry was prepared by suspended it (2 mg) in a mixture of 950 μL ethanol and ultrapure water by ultrasonication for 2 h. Finally, 5 μL slurry was drop-coated on the GCE surface and dried to obtain the modified GCE electrode.

1.4 Apparatus

The products were explored by an X-ray diffractometer (XRD, Bruker D8 Advance) with Co $\text{K}\alpha$ radiation (1.5418 Å, 40 kV and 40 mA). The sample morphology was visualized by field-emission scanning electron microscope (FE-SEM; Zeiss Gemini 300). Transmission electron microscopy (TEM), high-resolution TEM (HR-TEM), high-angle annular dark-field scanning transmission electron microscope (HAADF-STEM), and the corresponding energy dispersive X-Ray (EDX) mapping analyses (JEM-2100F, operated at 200 kV) were used to analyze morphology and structure of samples. X-ray photoelectron spectra (XPS) analysis carried out on an ESCALab 250XI electron spectrometer with an Al $\text{K}\alpha$ X-ray source (1486.6 eV). N_2 adsorption and desorption

analysis were performed on a Micromeritics ASAP 2460 adsorption instrument at 77 K with the Brunauer–Emmett–Teller (BET) method to calculate the specific surface area. X-ray absorption fine structure (XAFS) analyses of Ni and Co K-edge was performed with Si(111) crystal monochromators at the BL11B beamlines at the Shanghai Synchrotron Radiation Facility (SSRF) (Shanghai, China). Before the analysis at the beamline, samples were pressed into thin sheets with 1 cm in diameter and sealed using Kapton tape film. The XAFS spectra were recorded at room temperature using a 4-channel Silicon Drift Detector (SDD) Bruker 5040. Ni and Co K-edge extended X-ray absorption fine structure (EXAFS) spectra were recorded in transmission mode. Negligible changes in the line-shape and peak position of Ni and Co K-edge XANES spectra were observed between two scans taken for a specific sample. The XAFS spectra of these standard samples (Ni foil, NiO, Co foil, CoO, and Co₃O₄) were recorded in transmission mode. The obtained XAFS data was processed in Athena (version 0.9.26) for background, pre-edge line and post-edge line calibrations. Then Fourier transformed fitting was carried out in Artemis (version 0.9.26). The k^3 weighting, k -range of 3 – $\sim 12.5 \text{ \AA}^{-1}$ and R range of 1 – 3 \AA were used for the fitting of Co foil and Ni foil, respectively; the k^3 weighting, k -range of 3 – 11 \AA^{-1} and R range of 1 - 3 \AA were used for the fitting of samples. The four parameters, coordination number, bond length, Debye-Waller factor and E_0 shift (CN , R , ΔE_0) were fitted without anyone was fixed, the σ^2 was set. For Wavelet Transform analysis, the $\chi(k)$ exported from Athena was imported into the Hama Fortran code. The parameters were listed as follow: R range, 0 - 4 \AA , k range, 0 - 14 \AA^{-1} for samples; k weight, 3; and Morlet function with $\kappa=10$, $\sigma=1$ was used as the mother wavelet to provide the overall distribution. A CHI760E electrochemical workstation (Shanghai CH Instruments Co., China) is employed for electrochemical measurements with a standard three-electrode system, including a modified GCE working electrode, Ag/AgCl reference electrode, and Pt counter electrode.

1.5 DFT calculation

Periodic density functional theory (DFT) calculations are carried out by Vienna *ab initio* Simulation Package (VASP 5.4.1) within the generalized gradient approximation (GGA)^{3, 4}. The Perdew, Burke, and Ernzerhof (PBE) exchange-correlation functional was employed, and the

electron–ion interactions are represented by projected augmented wave (PAW) method^{5, 6}. The cut-off value of kinetic energy of plane wave group is 400 eV. To achieve faster convergence speed, the Gaussian smearing method with electron temperature of $k_B T = 0.05$ eV is adopted. A five-atomic-layer slabs with a (3×2) super unit cell is used to simulated the CoP (111) structure (Co:P=1:1). Some Co atoms were replaced by Ni atoms to form CoP-NiCoP and NiCoP structure. The ratio of Ni: Co: P on the surface of CoP-NiCoP and NiCoP is 3:9:12 and 6:6:12, respectively. These model systems top two layers are relaxed, while the bottom other layers in their optimized bulk locations are settled. It is assumed that along the normal direction (z) there is a vacuum space of 15 Å between the periodic slab models to avoid false interaction. The calculations use the Monkhorst Pack mesh k-points of $(2 \times 2 \times 1)$ via permitting convergence to 1×10^{-5} eV and below 0.05 eV/Å for total electronic energy as well as remaining total force, respectively. The adsorption energy of HQ and CC on different model systems is as follows: $\Delta E_{\text{ads}} = E_{\text{adsorbate+surface}} - (E_{\text{adsorbate}} + E_{\text{surface}})$, where $E_{\text{adsorbate+surface}}$ represent system total energy, E_{surface} is clean surface energy of different model systems, and $E_{\text{adsorbate}}$ is isolated HQ and CC energy. Transition state structures are received via climbing image nudged elastic band method (CI-NEB)⁷. To determine its characteristics (minimum or saddle point) for each optimized stationary point, vibrational analysis is conducted at the same theoretical level. The activation energy (E_a) of dissociation reaction is the initial and transition states energy differences.

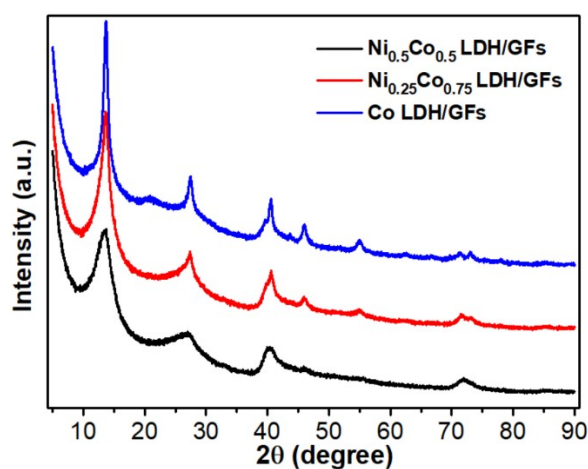


Fig. S1 XRD patterns of $\text{Ni}_{0.5}\text{Co}_{0.5}$ LDH/GFs, $\text{Ni}_{0.25}\text{Co}_{0.75}$ LDH/GFs, and Co LDH/GFs, respectively.

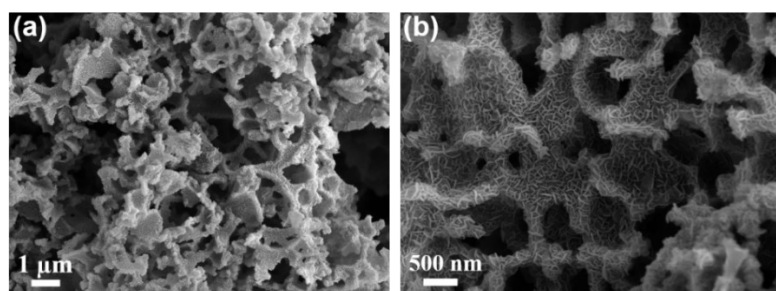


Fig. S2 (a) and (b) SEM images of $\text{Ni}_{0.25}\text{Co}_{0.75}$ LDH/GFs.

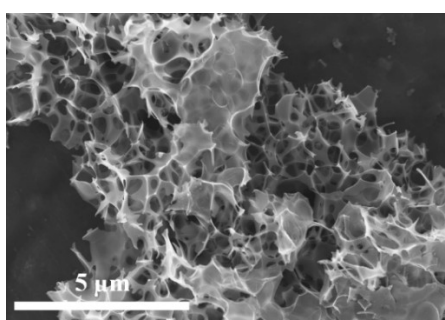


Fig. S3 SEM image of GFs.

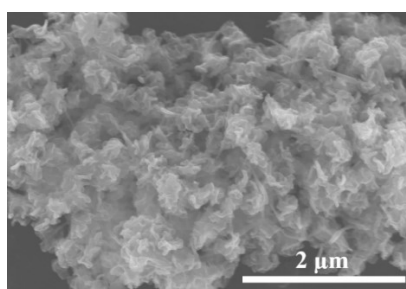


Fig. S4 SEM image of CoP-NiCoP.

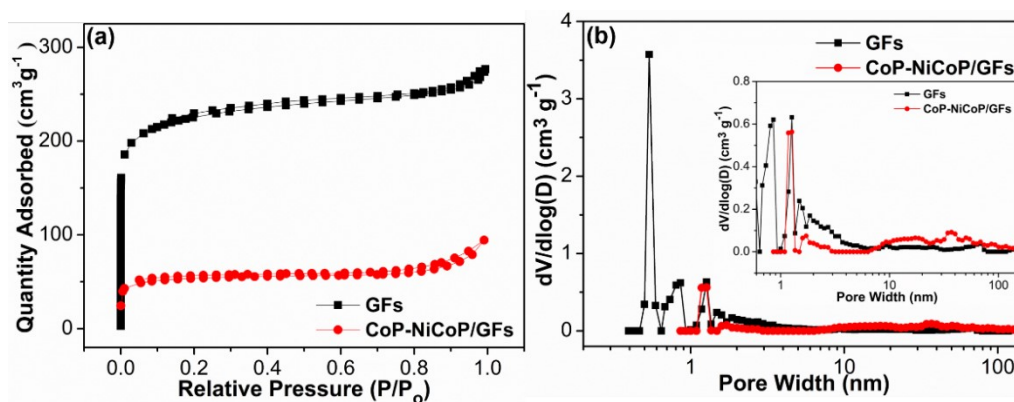


Fig. S5 N_2 adsorption-desorption isotherm and (b) pore size distribution curve of GFs and CoP-NiCoP/GFs, respectively.

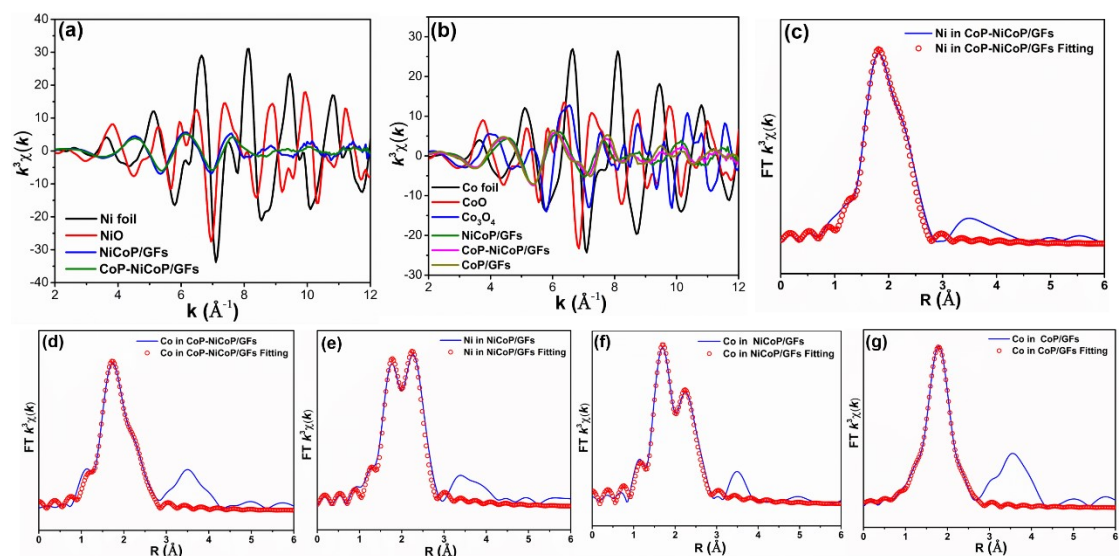


Fig. S6 (a, b) EXAFS in k -space, and the corresponding EXAFS fitting curves at R space for NiCoP/GFs (c, d), NiCoP/GFs (e, f), and CoP/GFs(g).

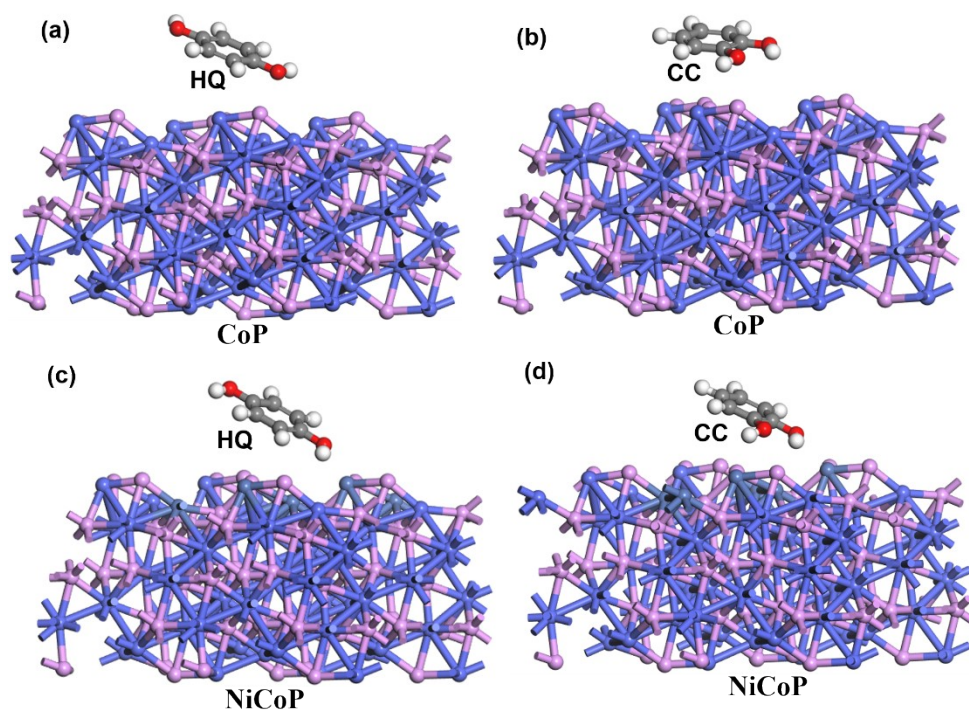


Fig. S7 The optimized HQ and CC adsorption configurations of (a) and (b) for CoP, (c) and (d) for NiCoP, respectively. In these models, the pink, blue, dark blue, white, red, and grey balls are referred to P, Co, Ni, H, O, and C, respectively.

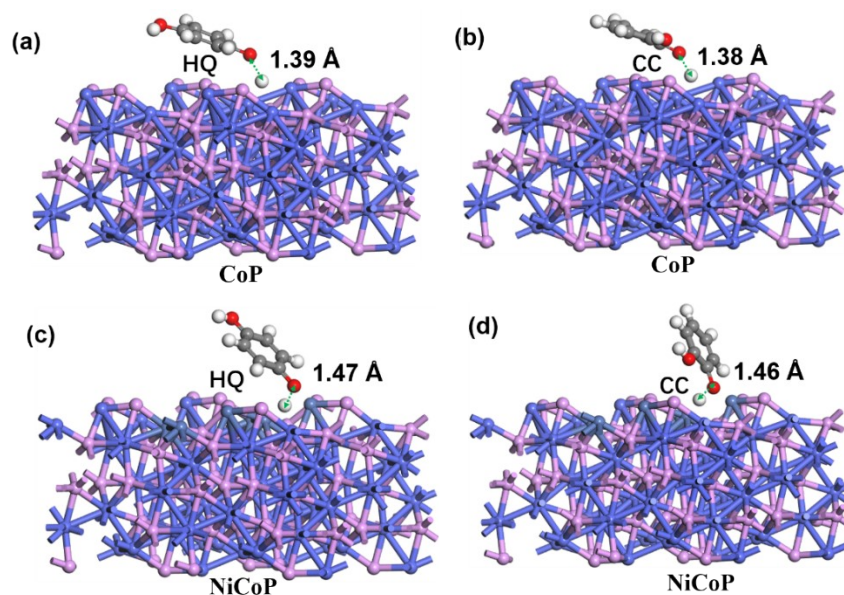


Fig. S8 The optimized hydrogen dissociation configurations of (a) and (b) for CoP, (c) and (d) for NiCoP, toward HQ and CC respectively. In these models, the pink, blue, dark blue, white, red, and grey balls are referred to P, Co, Ni, H, O, and C, respectively.

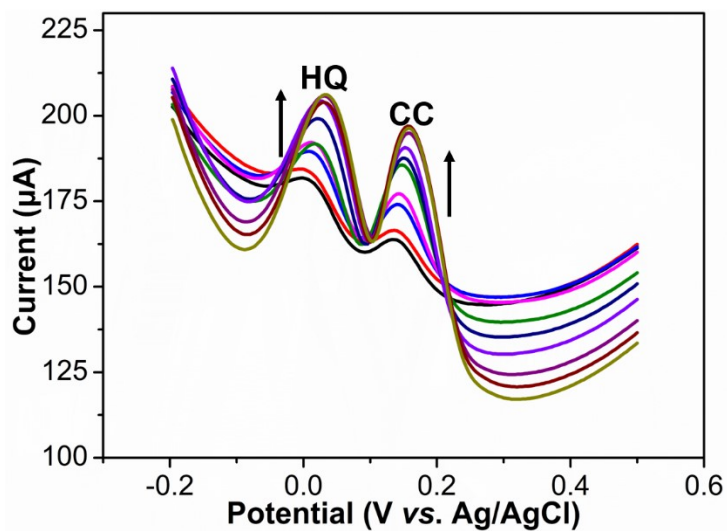


Fig. S9 DPV current responses curves of CoP-NiCoP/GFs based electrochemical sensor to detect various concentrations of HQ and CC ranging from 2-502 μM in 0.1 M PBS (pH 7.4).

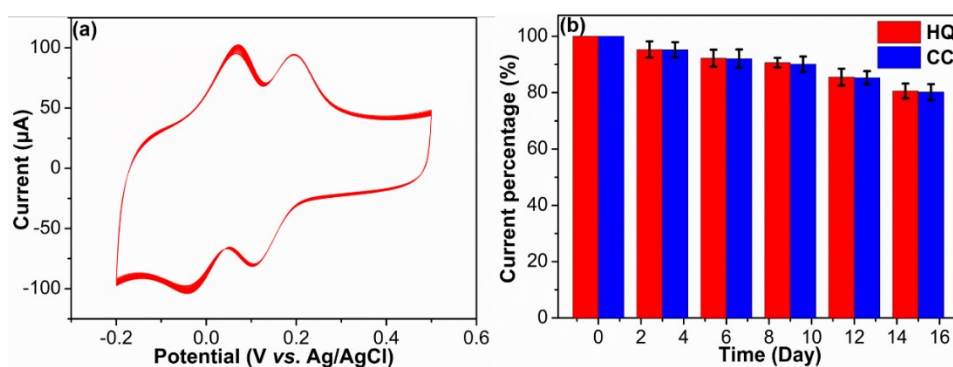


Fig. S10 (a) The CV curves of CoP-NiCoP/GFs modified electrode with 100 μM HQ and CC in 0.1 M PBS (pH=7.4) at a scan rate of 50 mV s^{-1} , (b) the relative current percentage of the CoP-NiCoP/GFs modified electrode toward 100 μM HQ and CC in 0.1 M PBS (pH=7.4) within 15 days.

Table S1 Structural parameters extracted from the EXAFS fitting.

Sample	Shell	CN	$R(\text{\AA})$	σ^2	ΔE_0	R factor
NiCoP/GFs	Co-P	3.3 ± 0.1	2.21 ± 0.01	0.0053	-4.9 ± 0.9	0.0045
	Co-Ni/Co	3.3 ± 0.1	2.58 ± 0.01	0.0068		
CoP-NiCoP/GFs	Co-P	3.6 ± 0.1	2.22 ± 0.01	0.0066	-7.7 ± 0.8	0.0027
	Co-Ni/Co	3.5 ± 0.2	2.56 ± 0.01	0.0100		
CoP/GFs	Co-P	4.5 ± 0.2	2.24 ± 0.01	0.0088	-6.4 ± 1.0	0.0014
	Co-Co	6.0 ± 0.5	2.58 ± 0.01	0.0194		
NiCoP/GFs	Ni-P	2.6 ± 0.2	2.25 ± 0.01	0.0057	-1.5 ± 1.3	0.0100
	Ni-Co/Ni	3.0 ± 0.2	2.60 ± 0.01	0.0064		
CoP-NiCoP/GFs	Ni-P	2.2 ± 0.1	2.23 ± 0.01	0.0049	-4.9 ± 1.5	0.0064
	Ni-Co/Ni	3.1 ± 0.2	2.55 ± 0.01	0.0096		

Table S2 The adsorption energy and H dissociation energy data over CoP, NiCoP, and CoP-NiCoP toward HQ and CC.

	Adsorption Energy (eV)		H dissociation energy (eV)	
	HQ	CC	HQ	CC
CoP	-0.04	-0.05	0.95	1.15
NiCoP	-0.22	-0.18	0.82	0.93
CoP-NiCoP	-0.28	-0.22	0.81	0.92

Table S3 Recovery results of HQ and CC in local river water based on CoP-NiCoP/GFs modified electrode (n=3), and n represents average of three determinations.

Analyte	Added (μM)	Found (μM)	Recovery (%)	RSD (%)
HQ	10	9.65	96.5	2.3
	20	20.22	101.1	3.1
	30	29.36	97.8	2.8
CC	10	10.15	101.5	2.7
	20	19.72	98.6	2.2
	30	30.37	101.2	2.7

Reference

1. Y. Zhu, K. Kang, Y. Jia, W. Guo and J. Wang, *Microchim. Acta*, 2020, **187**, 669.
2. R. Boppella, J. Tan, W. Yang and J. Moon, *Adv. Funct. Mater.*, 2019, **29**, 1807976.
3. G. Kresse and J. Hafner, *Phys. Rev. B*, 1994, **49**, 14251-14269.
4. G. Kresse and J. Furthmüller, *Comput. Mater. Sci.*, 1996, **6**, 15-50.
5. J. P. Perdew, K. Burke and M. Ernzerhof, *Phy. Rev. Lett.*, 1996, **77**, 3865-3868.
6. P. E. Blöchl, *Phys. Rev. B: Condens. Matter.*, 1994, **50**, 17953-17979.
7. G. Henkelman and H. Jónsson, *J. Chem. Phys.*, 2000, **113**, 9978-9985.